Inorganic Chemistry

Article

pubs.acs.org/IC

Assembly, Structure, and Reactivity of Cu_4S and Cu_3S Models for the Nitrous Oxide Reductase Active Site, Cu_Z*

Brittany J. Johnson,[†] Sergey V. Lindeman,[‡] and Neal P. Mankad*,[†]

[†]Department of Chemistry, University of Illinois at Chicago, 845 West Taylor Street, Chicago, Illinois 60607, United States

[‡]Department of Chemistry, Marquette University, 535 North 14th Street, Milwaukee, Wisconsin 53201, United States

Supporting Information

ABSTRACT: Bridging diphosphine ligands were used to facilitate the assembly of copper clusters with single sulfur atom bridges that model the structure of the Cu_Z* active site of nitrous oxide reductase. Using bis(diphenylphosphino)-amine (dppa), a $[Cu^I_4(\mu_4\text{-S})]$ cluster with N−H hydrogen bond donors in the secondary coordination sphere was assembled. Solvent and anion guests were found docking to the N−H sites in the solid state and in the solution phase, highlighting a kinetically viable pathway for substrate introduction to the inorganic core. Using bis-(dicyclohexylphosphino)methane (dcpm), a $[Cu^I_3(\mu_3\text{-S})]$ cluster was assembled preferentially. Both complexes exhibited reversible oxidation events in their cyclic voltammograms, making them functionally relevant to the Cu_Z* active site that is capable of catalyzing a multielectron redox transformation, unlike the previously known $[Cu^I_4(\mu_4\text{-S})]$ complex from Yam and co-workers supported by bis(diphenylphosphino)methane (dppm). The dppa-supported $[Cu^I_4(\mu_4\text{-S})]$ cluster reacted with N_3^-, a linear triatomic substrate isoelectronic to N_2O, in preference to NO_2^-, a bent triatomic. This $[Cu^I_4(\mu_4\text{-S})]$ cluster also bound I^-, a known inhibitor of Cu_Z*. Consistent with previous observations for nitrous oxide reductase, the tetracopper model complex bound the I^- inhibitor much more strongly and rapidly than the substrate isoelectronic to N_2O, producing unreactive μ_3-iodide clusters including a $[Cu_3(\mu_3\text{-S})(\mu_3\text{-I})]$ complex related to the $[Cu_4(\mu_4\text{-S})(\mu_2\text{-I})]$ form of the inhibited enzyme.

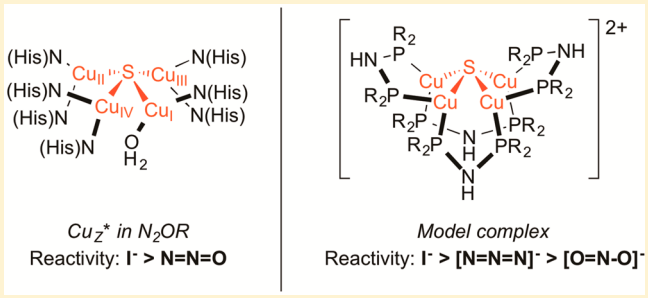

INTRODUCTION

Nitrous oxide (N_2O), a potent greenhouse gas and ozone layer depletion agent, is consumed in nature by nitrous oxide reductase (N_2OR) during bacterial denitrification.[1] N_2O activation and reduction occurs at a tetracopper sulfide active site within N_2OR, whose workings remain unclear. Two forms of this cluster have been characterized (Scheme 1a): one with a $[Cu_4(\mu_4\text{-S})]$ stoichiometry called Cu_Z*[2] and one with a $[Cu_4(\mu_4\text{-S})(\mu_2\text{-S})]$ stoichiometry called Cu_Z.[3] Although both Cu_Z* and Cu_Z have been proposed as the active form in nature, recent studies indicate that only Cu_Z* in its Cu^I_4 oxidation state is kinetically competent to mediate the two-electron reduction of N_2O under catalytically relevant conditions.[4] However, little is known about the intimate workings of Cu_Z* outside of computational studies,[5] and studies on the enzyme itself are complicated by the fact that purified N_2OR invariably contains mixtures of Cu_Z and Cu_Z*.[4] As a result, spectroscopic data on the active, fully reduced Cu_Z* are largely absent despite copious available data on other Cu_Z* oxidation states.[1,4] Inorganic model studies could, in principle, lend further understanding from experimental data related to cluster assembly, redox behavior, spectroscopic features, and chemical reactivity and mechanism. However, such studies are hindered by the fact that the structural motif present in Cu_Z* is unique in synthetic coordination chemistry. The only $[Cu_xS_y]$ cluster ever reported to exhibit N_2O reactivity does not reproduce the $[Cu_4S_1]$ stoichiometry in Cu_Z*,[6] limiting the insight that can be gained. In fact, not only do complexes with $[Cu_4(\mu_4\text{-S})]$ cores have almost no precedent, but more generally the rational construction of copper-containing clusters with *single* sulfur atom bridges remains a synthetic challenge.[7] Much more common is the construction of copper clusters bridged by *multiple* sulfur atoms, for example, with $[Cu_3S_2]$, $[Cu_{12}S_6]$, $[Cu_{13}S_2]$, or $[Cu_{20}S_{10}]$ cores, that bear little resemblance to Cu_Z* or other bioinorganic active sites.[8,9]

The complex $[(\mu_2\text{-dppm})_4Cu_4(\mu_4\text{-S})]^{2+}$ [**1**; dppm = bis-(diphenylphosphino)methane; see Scheme 1] represents the only known example of a synthetic $[Cu_4(\mu_4\text{-S})]$ cluster prior to this report.[10] This complex has been studied in great detail for its optical properties but is limited in its ability to serve as a functional model for Cu_Z*.[11] Not only is air-stable **1** relatively inert in nature, but also it does not exhibit the reversible electrochemistry necessary to model a bioinorganic active site, such as Cu_Z*, that mediates a multielectron redox transformation. Some of these drawbacks in the ability of **1** to model Cu_Z* may stem from its use of phosphorus donors, as opposed to the nitrogen donors of Cu_Z*, to stabilize the $[Cu_4(\mu_4\text{-S})]$

Received: July 17, 2014
Published: September 11, 2014

Scheme 1. (a) N_2O Reduction by Bioinorganic Copper Sulfide Clusters Cu_Z* and/or Cu_Z (His = Histidine) and (b) Synthetic Copper Sulfide Clusters Discussed in This Report

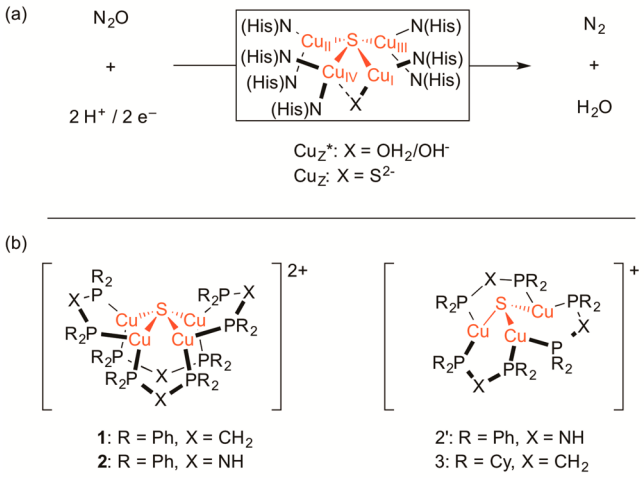

core. However, spectroscopic and computational analyses of Cu_Z* indicate that its redox-active molecular orbital is largely localized (83%) on the four copper centers and the bridging sulfur,[12] implying that the supporting nitrogen donors are limited in their orbital contributions to chemically relevant frontier orbitals. Computational analysis of **1** has similarly indicated that its redox-active molecular orbital is largely localized (84%) on the four copper centers and bridging sulfur.[13] Because of these similar electronic structures as well as the demonstrated, unique ability of dppm to control the Cu:S stoichiometry, we deemed that derivatives of complex **1** merited further examination.

Fortunately, the bridging diphosphine ligands in use for constructing **1** are readily tuned to overcome these kinetic and thermodynamic shortcomings. In this contribution, we report the synthesis and characterization of new copper monosulfide clusters ($[(\mu_2\text{-dppa})_4Cu_4(\mu_4\text{-S})][PF_6]_2$ (**2**) and $[(\mu_2\text{-dcpm})_3Cu_3(\mu_3\text{-S})][PF_6]\cdot OCMe_2$ (**3**); see Scheme 1) that assemble to model structural features relevant to the $[Cu_4S]$ core of Cu_Z*, including the presence of hydrogen-bond donors in the secondary coordination sphere. These complexes also exhibit reversible electrochemistry, and one (**2**) also presents chemical reactivity toward a substrate that is isoelectronic to N_2O, azide (N_3^-), and toward a known inhibitor of the N_2OR enzyme, iodide (I^-). Competition experiments reveal that the linear triatomic, N_3^-, binds more rapidly than a bent triatomic,

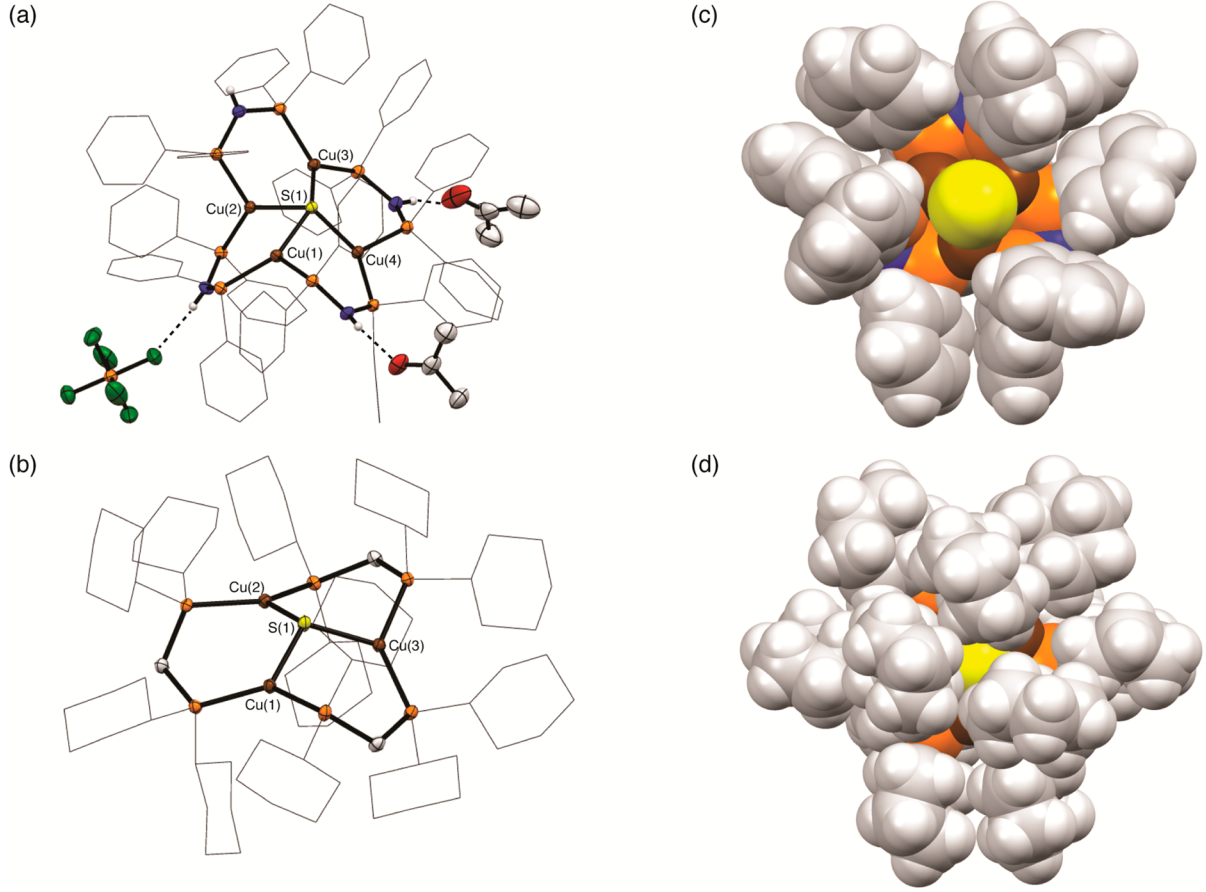

Figure 1. Solid-state structures of (a) **2**·2$OCMe_2$ and (b) **3** determined by X-ray crystallography. Core atoms are shown as 50% probability ellipsoids, phosphine substituents are shown as wireframes, and C−H hydrogen atoms have been omitted for clarity. Cocrystallized anions and solvent molecules are shown only if engaged in hydrogen bonding to the cationic unit. N−H hydrogen atoms are shown in calculated positions. Space-filling models of the cationic portions of (c) **2′** and (d) **3**, both based on crystallographically determined coordinates and viewed down the sulfur (pseudo-)C_3 axis, with all hydrogen atoms shown in calculated positions. Atom colors: C, gray; H, white; Cu, brown; F, green; N, blue; O, red; P, orange; S, yellow.

dx.doi.org/10.1021/ic501720h | *Inorg. Chem.* 2014, 53, 10611−10619

nitrite (NO_2^-), but much less rapidly than the enzyme inhibitor, I^-.

RESULTS AND DISCUSSION

Cluster Assembly and Structure. One design strategy we chose to pursue involved modifying dppm-supported **1** to include hydrogen-bond donors in the secondary coordination sphere. It is well recognized that secondary-sphere hydrogen-bonding interactions are crucial to the design of functional models of metalloenzymes.[14] Building such a model for Cu_Z* could, in principle, provide kinetically viable pathways for the introduction of substrates to the inorganic [$Cu_4(\mu_4$-S)] core. Indeed, for N_2OR itself, it is thought that hydrogen bonding from the N−H groups of lysine and histidine residues located nearby to the Cu_Z* cluster may assist in N_2O binding and subsequent N_2 extrusion.[5,15] In order to construct a copper sulfide cluster with hydrogen-bond donors, we targeted the use of bis(diphenylphosphino)amine (dppa) in place of dppm. The second strategy we chose to pursue involved modifying **1** to render the copper sulfide core more electron-rich, with the goal of stabilizing higher oxidation states and thereby obtaining reversible electrochemistry. In order to construct a more electron-rich copper sulfide cluster, we targeted the use of bis(dicyclohexylphosphino)methane (dcpm) in place of dppm.

The slow addition of a methanolic solution of Na_2S (0.5 equiv) to an acetone solution of colorless [$(\mu_2$-dppa)$_2$Cu$_2$(NCCH$_3$)$_2$][PF$_6$]$_2$[16] produced a rapid color change to bright orange. Slow diffusion of diethyl ether vapors into the acetone solution produced **2** as pale-orange plates. Combustion analysis of these plates, upon crushing and drying, was consistent with the dicationic tetracopper formulation. X-ray diffraction analysis of one of the plates confirmed the assembly of a [$Cu_4(\mu_4$-S)] core stabilized by four bridging dppa ligands, along with the presence of two PF_6^- counterions per tetracopper cluster. Additionally, we believe that a minor fraction of the product mixture was the tricopper species [$(\mu_2$-dppa)$_3$Cu$_3$(μ_3-S)][PF$_6$] (**2′**) because a single crystal of that species also was identified among the sample and analyzed by X-ray diffraction (see Figures S44 and S45 in the Supporting Information, SI). However, no spectroscopic evidence for the formation of **2′** was obtained, indicating that it is formed only in trace amounts under these reaction conditions.

The core structure of **2** is shown in Figure 1a. Unlike **1**, which features a relatively symmetric [$Cu_4(\mu_4$-S)] core [neighboring Cu···Cu distances of 2.869(1)−3.129(1) Å],[10] the inorganic core of **2** is asymmetric. While three of the copper centers in **2** are close together [Cu(1)···Cu(2), 2.6571(7) Å; Cu(2)···Cu(3), 2.7184(4) Å], a fourth copper center is significantly displaced from the others [Cu(4)···Cu(1), 3.1005(5) Å; Cu(4)···Cu(3), 3.5365(6) Å]. Two acetone solvent molecules and a PF_6^- anion engage in hydrogen bonding with N−H groups in the secondary coordination sphere. The two acetone molecules are associated with the N−H residues of the two bridging dppa ligands directly bound to Cu(4), in essence "pulling" Cu(4) away from the rest of the cluster (Figure 1a). Such a phenomenon is impossible for **1**, which lacks any hydrogen-bond donors. Similar hydrogen-bonding motifs have been noted for [$(\mu_2$-dppa)$_3$Cu$_3$(μ_3-SH)$_2$][BF$_4$].[17] The environment of the sulfur center in **2** is best described as a seesaw shape (τ_4 = 0.64).[18]

The structural parameters within the [$Cu_4(\mu_4$-S)] cores of Cu_Z*, Cu_Z, **1**, and **2** are compared in Table 1. The distorted core in **2** accesses a relatively large span of Cu···Cu distances,

Table 1. Structural Comparisons of Cu_Z*, Cu_Z, 1, and 2

parameter	Cu_Z*[a]	Cu_Z[b]	1[c]	2
Cu···Cu (Å)	2.54[d]	2.83[d]	2.869(2)[d]	2.6571(7)[d]
	2.56[d]	2.84[d]	2.869(2)[d]	2.7184(4)[d]
	3.00[d]	2.95[d]	3.128(1)[d]	3.1005(5)[d]
	3.33[d]	3.38[d]	3.128(1)[d]	3.5365(6)[d]
	3.36[e]	3.41[e]	4.169(2)[e]	3.9697(6)[e]
	4.43[e]	4.60[e]	4.303(1)[e]	4.2857(6)[e]
Cu−μ_4-S (Å)	2.09	2.19	2.267(1)	2.2452(6)
	2.16	2.22	2.267(1)	2.2619(8)
	2.21	2.35	2.269(2)	2.2418(7)
	2.25	2.44	2.269(2)	2.2217(8)
τ_4[f]	0.66	0.71	0.59	0.64

[a]From analysis of the coordinates from PDB accession code 1QNI. See ref 2. [b]From analysis of the coordinates from PDB accession code 3SBR. See ref 3. [c]Duplicate values from crystallographic symmetry equivalence. See ref 10. [d]Neighboring Cu···Cu distance. [e]Cross-cluster Cu···Cu distance. [f]τ_4 value of the μ_4-sulfur. See ref 18.

making it the most accurate model of the distorted core in Cu_Z* reported to date. As judged by τ_4 values, the μ_4-sulfide ligands in all of the tetracopper clusters have seesaw geometries, with the τ_4 values for **1** and **2** more closely matching Cu_Z* than Cu_Z. These τ_4 values further confirm that **2** contains a more structurally faithful inorganic core model of Cu_Z* at the sulfur bridge, which may play an important role in N_2O docking in N_2OR.[5]

In addition to the hydrogen-bonding interactions observed in the solid-state structure of **2**, they appear to be present in the solution phase, as well. First, solutions of **2** are air-sensitive, unlike solutions of **1**, which may imply that the N−H groups play a role in transporting O_2 from air to the [$Cu_4(\mu_4$-S)] core of **2**.[19] Second, the ^{31}P NMR spectra of **2** were highly solvent-dependent. A sample of **2** that had been synthesized in and crystallized from acetone, and therefore was expected to have acetone guests docked to the ligand periphery, exhibited a single broad ^{31}P NMR resonance in acetone-d_6 at 36.6 ppm. Dissolving the same sample in acetonitrile-d_3 resulted in two sharper ^{31}P NMR resonances at 36.8 and 36.5 ppm, respectively. Thinking that the 36.8-ppm signal corresponded to a species where acetone guest molecules had been displaced by acetonitrile guest molecules, we then conducted the synthesis and precipitation of **2** in acetonitrile. Analyzing this sample in acetonitrile-d_3 revealed a single sharp ^{31}P NMR resonance at 36.8 ppm. A similar phenomenon was observed with dimethyl sulfoxide-d_6. Collectively, these data (Figure 2) provide clear evidence that the docking of solvent molecules to the periphery of **2** via hydrogen bonding is a phenomenon that exists in the solution phase and that exchange of the guest molecules can occur at ambient conditions.

The addition of Na_2S (0.5 equiv) to [$(\mu_2$-dcpm)$_2$Cu$_2$][PF$_6$]$_2$[20] resulted in incomplete conversion to a new species, as judged by NMR spectroscopy. Complete conversion to the new species only was attained when 0.67 equiv of Na_2S was used. Consistent with this stoichiometry, crystallization of the product by slow diffusion of diethyl ether vapors into an acetone solution provided pale-yellow crystals of **3**. X-ray diffraction analysis confirmed the monocationic tricopper formulation and revealed a [$Cu_3(\mu_3$-S)] core that has limited precedent in the literature (Figure 1b).[7a,b] Presumably, the bulkier cyclohexyl substituents preclude the formation of a tetracopper cluster and preferentially direct the assembly of a

dx.doi.org/10.1021/ic501720h | Inorg. Chem. 2014, 53, 10611−10619

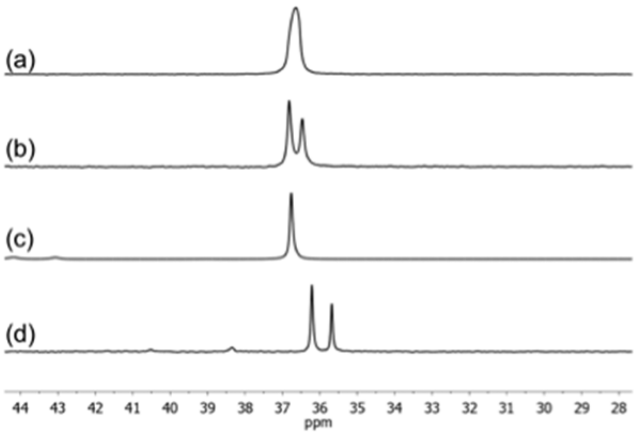

Figure 2. ^{31}P NMR spectra of **2** in (a) acetone-d_6 after preparation in acetone, (b) acetonitrile-d_3 after preparation in acetone, (c) acetonitrile-d_3 after preparation in acetonitrile, and (d) dimethyl sulfoxide-d_6 after preparation in acetone.

tricopper core in order to ease steric congestion. Accordingly, the Cu···Cu distances in **3** [3.5684(3)−3.6753(3) Å] are significantly longer than those in **1** and **2**. Parts c and d of Figure 1 compare space-filling models of $[Cu_3S]$ complexes **2′** and **3**, further highlighting the increased steric congestion imparted by dcpm. The geometry of the sulfur center in **3** is trigonal-pyramidal with approximate C_3 symmetry [Cu−S−Cu angles: 107.61(2)−111.78(2)°]. Complex **3** complements the recent characterization of a $[Cu_3(\mu_3\text{-}S)]$ cluster by Murray and co-workers,[7a] which features a planar rather than pyramidal S^{2-} ligand and was characterized in higher oxidation states ($Cu^{II}Cu^{II}Cu^{I}$ and $Cu^{II}Cu^{I}Cu^{I}$) than **3** ($Cu^{I}Cu^{I}Cu^{I}$), possibly because of the use of hard nitrogen ligands instead of soft phosphorus ligands to support the cluster.

Electrochemical and Photophysical Characterization. The N_2OR enzyme catalyzes a multielectron redox transformation, implying that the Cu_Z* active site can stabilize multiple redox states. Accordingly, any functional model of Cu_Z* should exhibit reversible electrochemical behavior. The dppm complex, **1**, was reported previously to have three ill-defined, irreversible oxidation events with onset at 0.27 V versus $[FeCp_2]^{+/0}$.[10] Analysis of the dppa analogue, **2**, instead revealed a reversible oxidation event by cyclic voltammetry (CV), cathodically shifted to −0.12 V (Figure 3a), followed by three ill-defined, irreversible oxidation events (Table 2 and Figure S1 in the SI). The significant cathodic shift resulting from substituting dppm with the more strongly donating dppa is well precedented in various coordination complexes.[21] The dcpm analogue, **3**, also exhibited a fully reversible oxidation event in its CV, further cathodically shifted to −0.35 V (Figure 3b), followed by three irreversible oxidations (Table 2 and Figure S4 in the SI). Assuming that each copper center can access the Cu^{I} and Cu^{II} states only, the presence of four oxidation events for the tricopper complex, **3**, implies that the μ_3-S^{2-} ligand also participates in oxidation chemistry. Such noninnocent behavior of bridging sulfur atoms is well documented through spectroscopic and computational analyses of dicopper complexes with bridging $[(S)_2]^{n-}$ units.[22] For comparison to the data reported here, a lower limit can be placed on the $Cu^{II}Cu^{I}{}_3/Cu^{I}{}_4$ potential of Cu_Z* based on the fact that methyl viologen is required to access the fully reduced state.[4] Using the reduction potential of methyl viologen[23] as a lower limit and converting from the SCE scale to the

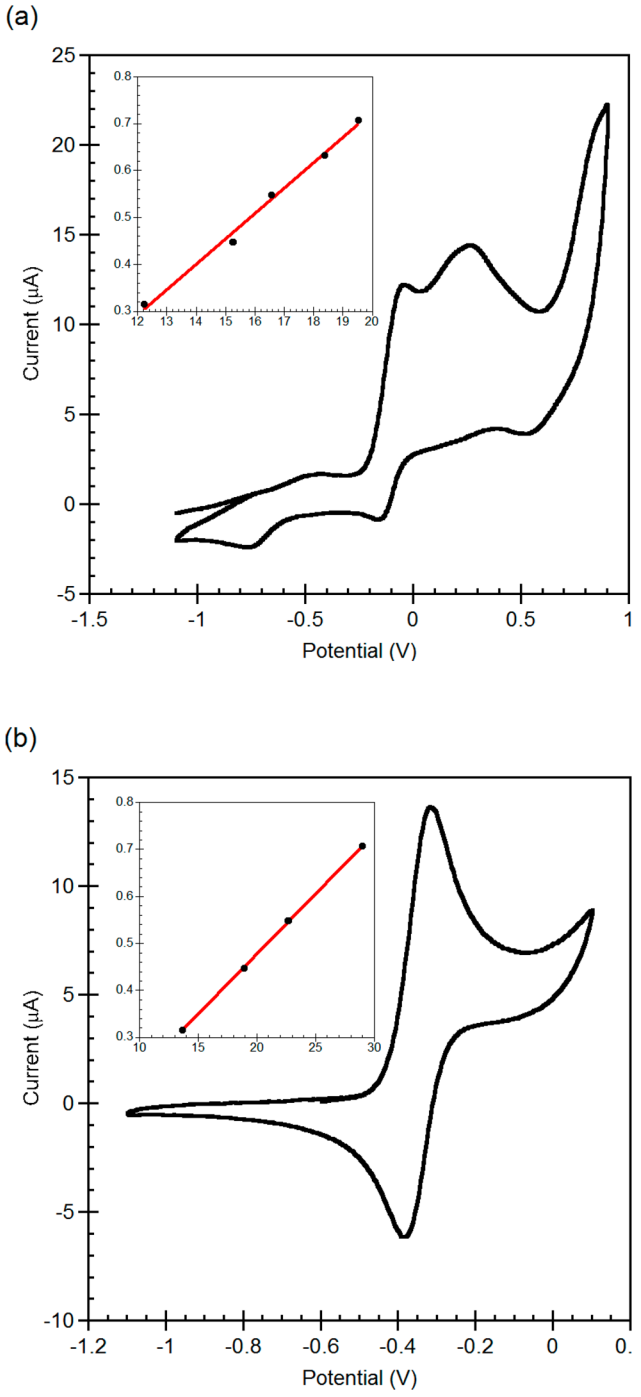

Figure 3. Cyclic voltammograms of (a) **2** and (b) **3** in CH_3CN (0.1 M Bu_4NPF_6, 100 mV s^{-1} scan rate, Pt working electrode). Potentials are referenced to $[FeCp_2]^{+/0}$. Insets: Plots of the square root of the scan rate (V s^{-1}) versus current (μA) in the forward direction for the first oxidations. The linear dependence indicates reversible electrochemical behavior (R^2 = 0.99614 and 0.99993, respectively).

$[FeCp_2]^{+/0}$ scale using the method of Pavlishchuk and Addison,[24] we estimated the reduction potential of Cu_Z* as $E^0 > -0.78$ V versus $[FeCp_2]^{+/0}$.[25] While the precise reduction potential for Cu_Z* is not known, the model complexes in this work also fall above this lower limit.

In light of the noteworthy photophysical properties previously noted for **1**,[10] we examined the photophysical characteristics of **2** and **3** for comparison. The lowest-energy

dx.doi.org/10.1021/ic501720h | Inorg. Chem. 2014, 53, 10611−10619

Table 2. Electrochemical and Photophysical Properties of 1−3

property	1[a]	2	3
$E_{oxidation}$ (V)[b]	0.27, 1.25, 1.39	−0.12 (rev.),[c] 0.27, 0.88, 1.55	−0.35 (rev.),[c] 0.29, 0.86, 1.58
$\lambda_{emission}$ (nm)[d]	618	704	642
Φ[e]	0.22	0.067	0.0007

[a]From ref 10. [b]Referenced to $[FeCp_2]^{+/0}$, from CV in CH_3CN (0.1 M $[Bu_4N][PF_6]$, Pt working electrode, and 100 mV s^{-1} scan rate). [c]Reversible. [d]Emission measured with an excitation wavelength of 415 nm in CH_3CN at room temperature. [e]Quantum yield measured with an excitation wavelength of 415 nm in CH_3CN at room temperature for all compounds.

absorption of **1** is at 285 nm, a feature that shifts to 284 nm for **2** and 279 nm for **3**.[26] As expected, these fully reduced complexes lack any low-energy absorption in the 450−550 nm range observed for the resting, one-hole states of Cu_Z* and Cu_Z.[1] Like **1**, both **2** and **3** are luminescent and glow orange upon excitation. The emission wavelengths and quantum yields were ligand-dependent (Table 2). The quantum yield measured for **3** was significantly lower than those of **1** and **2**, indicating a special ability of the $[Cu_4(\mu_4\text{-}S)]$ motif to support efficient excited-state chemistry and bright emission.

Reactivity toward N_3^- and I^-. N_2O is notoriously inert toward inorganic systems. Very few transition-metal coordination complexes react with gaseous N_2O,[27] and fewer still of these systems also contain copper, a metal of low azo- and oxophilicity.[6,28] Accordingly, we have not observed any evidence by spectroscopic methods for reactivity between N_2O and **1**, **2**, or **3** under the reaction conditions we have screened thus far. However, we hypothesized that relevant reactivity would be observed with other triatomic substrates that, while closely related to N_2O in electronic structure, possess overall anionic charge. Particularly fascinating to us were azide (N_3^-), which is a linear triatomic anion, and nitrite (NO_2^-), which is a bent triatomic anion. Although N_2O is a linear triatomic molecule in its ground state, computational studies have suggested that significant N−N−O bending is observed during its binding to the Cu_Z* cluster in N_2OR.[5] In this regard, N_3^- resembles the ground-state geometry of N_2O, while NO_2^- resembles the transition state structure proposed for N_2O binding to Cu_Z*. We also chose to examine the chemistry of our model system **2** with iodide (I^-), a known inhibitor of N_2OR.[29]

Complex **2** reacted readily with excess NaN_3 at room temperature, producing a mixture of two complexes that were both identified crystallographically (Scheme 2). One of the products was the $[Cu_3(\mu_3\text{-}S)]$ complex, **2′**, and the second product was $[(\mu_2\text{-dppa})_3Cu_3(\mu_3\text{-}N_3)_2][PF_6]$ (**4**). Because of their similar solubility properties, we were not able to separate **2′** and **4**, which were produced in a ratio of 2.7:1 in the crude reaction mixture (Figures S22 and S23 in the SI). However, **4** was produced as the major copper-containing product from the reaction between **2** and N_3SiMe_3; this method provided us with pure samples of **4** for full characterization (Figures S24−S26 in the SI). The IR spectrum of **4** featured a characteristic azide vibration at 2046 cm^{-1}, shifted from 2103 cm^{-1} in NaN_3. The solid-state structure of **4** (Figure 4) featured three tetrahydrofuran (THF) molecules (the solvent of crystallization) bound to each of the three N−H groups in the secondary coordination sphere. The cationic portion of **4** possessed

Scheme 2. Reactivity of the $[Cu^I_4(\mu_4\text{-}S)]$ Cluster 2 with NaN_3 and NaI

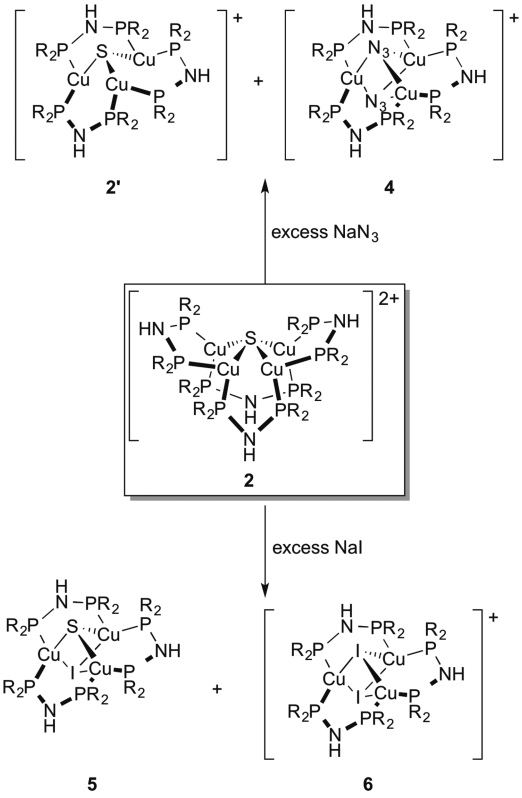

approximate C_3 symmetry, with the N_3 units deviating slightly from the C_3 axis. The end-on, μ_3 binding of N_3^- to the multicopper cluster contrasts with the proposed side-on binding of N_2O to Cu_Z*.[5] Under the same reaction conditions, $NaNO_2$ did not react with **2**.

Complex **2** also reacted readily with excess NaI at room temperature, producing a mixture of two new complexes that were each identified crystallographically (Scheme 2). One of the products was $[(\mu_2\text{-dppa})_3Cu_3(\mu_3\text{-}S)(\mu_3\text{-}I)]$ (**5**; Figure 4), and the second product was $[(\mu_2\text{-dppa})_3Cu_3(\mu_3\text{-}I)_2][PF_6]$ (**6**; Figure S46 in the SI). A toluene extraction was used to separate neutral **5** from cationic **6**, which were produced in a ratio of 1:5.8 in the crude reaction mixture (Figures S27−S31 in the SI). We suspect that Na_2S was a byproduct of this reaction, accounting for the displaced sulfide equivalents. The solid-state structures of both **5** and **6** featured roughly C_3-symmetric tricopper clusters. In the case of **6**, one THF molecule was found hydrogen bonding to a N−H group in the secondary coordination sphere. In the case of **5**, no such interactions were detected (Figure 4). Presumably, the N−H groups in **5** are less acidic because of the neutral charge of the complex and therefore do not engage as readily in hydrogen-bonding interactions. The crystal structure of N_2OR under iodide inhibition features an iodide-bound Cu_Z* cluster with a $[Cu_4(\mu_4\text{-}S)(\mu_2\text{-}I)]$ core that is related to the $[Cu_3(\mu_3\text{-}S)(\mu_3\text{-}I)]$ core found in **5**, although the Cu···μ_2-I distances observed in the enzyme are shorter (2.5 and 2.8 Å) than the Cu···μ_3-I distances observed in **5** [2.8632(12), 2.9390(14), and 2.9481(12) Å].[29] For comparison, the Cu···μ_3-I distances in **6** ranged from 2.7152(9) to 2.7608(8) Å.

In N_2OR, the Cu_Z* cluster is inhibited from reacting with its normal substrate, N_2O, when I^- is present. Similarly, model

dx.doi.org/10.1021/ic501720h | Inorg. Chem. 2014, 53, 10611−10619

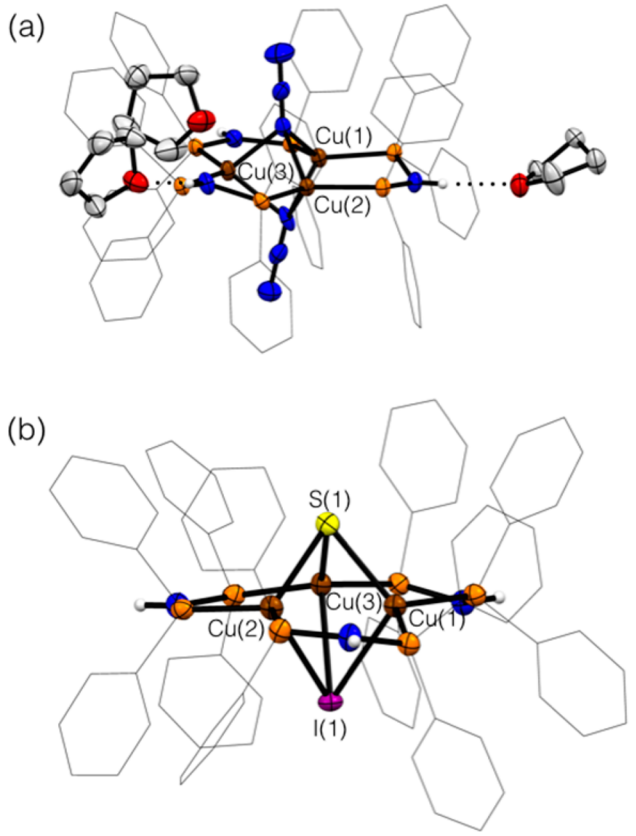

Figure 4. Solid-state structures of (a) **4**·3THF and (b) **5** determined by X-ray crystallography. Core atoms are shown as 50% probability ellipsoids, phosphine substituents are shown as wireframes, and C−H hydrogen atoms have been omitted for clarity. Cocrystallized anions and solvent molecules are shown only if engaged in hydrogen bonding to the cationic unit. N−H hydrogen atoms are shown in calculated positions. Atom colors: C, gray; H, white; Cu, brown; F, green; I, purple; N, blue; O, red; P, orange; S, yellow.

complex **2** is inhibited from reacting with N_3^- by the presence of I^-. Several experiments were used to establish this behavior. First of all, the reaction of **2** with a 1:1 mixture of NaI/NaN_3 produced **5** and **6** with no evidence for the formation of **2′** or **4** by ^{31}P NMR (Figures S33−S35 in the SI), indicating the strong kinetic preference for the I^- reaction with the $[Cu_4(\mu_4\text{-}S)]$ core over the N_3^- reaction. The reaction of **4** with excess NaI cleanly produced **6** (Figures S36−S38 in the SI), while no reaction was observed between NaN_3 and either **5** or **6** (Scheme 3 and

Scheme 3. Competitive Binding of I^- over N_3^-

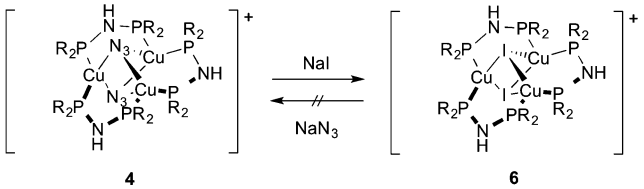

Figures S39−S41 in the SI). This set of experiments provides further indication that I^- binds strongly to the multicopper clusters and inhibits a reaction with an otherwise competent substrate, N_3^-, in analogy to Cu_Z* inhibition.

CONCLUSIONS

In conclusion, the self-assembly of $[Cu_n(\mu_n\text{-}S)]$ clusters structurally related to the Cu_Z* site of N_2OR was observed using bridging diphosphine supporting ligands. The identity of the diphosphine unit controlled the nature of the cluster that assembled, enabled tuning of thermodynamic reduction potentials of the clusters, and was used to introduce hydrogen-bond donors to the secondary coordination sphere of one model. Reactivity studies of this $[Cu^I_4(\mu_4\text{-}S)]$ model with various anions provided information related to the different binding preferences of such copper−sulfur clusters. Specifically, the reactivity data presented here indicate that the $[Cu^I_4(\mu_4\text{-}S)]$ model complex **2** binds anions in the following order of preference: $I^- > N_3^- > NO_2^-$. These reactions resulted in a breakdown of the tetracopper cluster to generate various tricopper clusters, in some cases with displacement of the sulfide unit. Such loss of nuclearity and stoichiometry is likely prevented for Cu_Z* by the rigid secondary structure provided by N_2OR,[1,5] highlighting an important challenge in modeling this fascinating active site. Further tuning of these clusters through the design of bridging diphosphine units will be pursued with emphasis on enabling reactivity with N_2O itself.

EXPERIMENTAL SECTION

General Considerations. Unless otherwise specified, all reactions and manipulations were performed under purified N_2 in a glovebox or using standard Schlenk-line techniques. Glassware was oven-dried prior to use. Acetone and methanol were degassed with N_2, dried over K_2CO_3, and then distilled and stored over activated 3-Å molecular sieves. Other reaction solvents (diethyl ether, toluene, tetrahydrofuran, and dichloromethane) were sparged with argon and dried using a Glass Contour Solvent System built by Pure Process Technology, LLC. Unless otherwise specified, all chemicals were purchased from commercial sources and used without further purification.

Physical Measurements. NMR spectra were recorded at ambient temperatures using a Bruker Avance DPX-400 or a Bruker Avance DRX-500 MHz spectrometer. ^1H NMR chemical shifts were referenced to residual solvent peaks. ^{31}P NMR chemical shifts were referenced to external H_3PO_4 ($\delta = 0$). The following data acquisition parameters were used for quantative ^{31}P NMR spectroscopy: single pulse, 8.00 μs; power level, −3.00 dB; frequency offset of the third nucleus, −748516.887 ppm; recycle delay, 10 s; number of scans, 128. The signal-to-noise ratio calculated for ^{31}P NMR using these parameters was 0.8%. Fourier transform infrared (FT-IR) spectra were recorded on solid samples in a glovebox using a Bruker ALPHA spectrometer fitted with a diamond-ATR detection unit. Elemental analyses were performed by the Midwest Microlab, LLC, Indianapolis, IN. Deuterated solvents were degassed by repeated freeze−pump−thaw cycles and then stored over 3-Å molecular sieves. UV−vis absorbance spectra were taken at room temperature using a Cary 300 Bio UV−vis spectrophotometer. Fluorescence emission spectra were taken at room temperature using a customized Fluorolog (Horiba Jobin Yvon) modular spectrofluorometer. Luminescence quantum yields were determined based on eq 1, where A is the measured absorbance at the excitation wavelength and I is the integrated emission intensity when samples were excited at 415 nm. A 7.10×10^{-4} M solution of compound **1** ($\Phi = 0.22$;[10] excitation wavelength = 415 nm) in MeCN was used as the standard reference solution. Samples for emission measurements were prepared as solutions of compounds **2** and **3**, in MeCN, at concentrations of 5.66×10^{-4} and 3.14×10^{-3} M, respectively.

$$\phi_{sample} = \phi_{reference} \frac{A_{reference}}{A_{sample}} \frac{I_{sample}}{I_{reference}} \quad (1)$$

Electrochemical data were measured at room temperature using a WaveNow USB potentiostat from Pine Research Instrumentation. In a

dx.doi.org/10.1021/ic501720h | Inorg. Chem. 2014, 53, 10611−10619

classic three-electrode system, a platinum working electrode, a platinum counter electrode, and a $Ag/AgNO_3$ (0.01 M $AgNO_3$/0.1 M Bu_4NPF_6 in MeCN) reference electrode were used. Compounds **2** and **3** were dissolved in a 0.1 M solution of Bu_4NPF_6 in MeCN at 1.88×10^{-3} M concentration. Electrochemical measurements were referenced to a 1.88×10^{-3} M solution of $FeCp_2^{+/0}$ in the same MeCN electrolyte solution.

X-ray Crystallography. X-ray crystallography data were collected at the X-ray Structural Laboratory at Marquette University (Milwaukee, WI) for complexes **2**, **2′**, **3**, **4**, and **5**. Single-crystal X-ray diffraction data were collected at 100 K with an Oxford Diffraction SuperNova κ diffractometer equipped with dual microfocus Cu/Mo X-ray sources, X-ray mirror optics, an Atlas CCD detector, and a low-temperature Cryojet device. The data were processed with the *CrysAlisPro* program package (Oxford Diffraction Ltd., 2010) typically using a numerical Gaussian absorption correction (based on the real shape of the crystal) followed by an empirical multiscan correction using the *SCALE3 ABSPACK* routine. The structures were solved using the *SHELXS* program and refined with the *SHELXL* program[30] within the *Olex2* crystallographic package.[31] All computations were performed on an Intel PC computer under Windows 7 OS. X-ray crystallography data were collected at the University of Illinois at Chicago for complex **6**. Single-crystal X-ray diffraction data were collected at 200 K with a Bruker SMART X2S benchtop diffractometer fitted with an Oxford Cryostreams Desktop Cooler. The structure was solved using *SHELXS* and refined with *SHELXL*.[30]

Most of the structures contain a certain degree of disorder, which was detected in difference Fourier syntheses of the electron density and was taken care of using the capabilities of the *SHELX* package. In most cases, hydrogen atoms were localized in difference syntheses of the electron density but were refined using appropriate geometric restrictions on the corresponding bond lengths and bond angles within a riding/rotating model (torsion angles of the Me hydrogen atoms were optimized to better fit the residual electron density). The particular nonstandard details of the structure solution and refinement are as indicated in the figure captions included as SI.

Preparation of Bis(diphenylphosphino)amine (dppa). A literature procedure was adapted for the isolation of dppa.[32] Toluene (30 mL), chlorodiphenylphosphine (3.30 mL, 18.4 mmol), and hexamethyldisilazane (1.92 mL, 9.23 mmol) were added sequentially to a 100 mL three-necked round-bottom flask inside a glovebox. Upon the addition of hexamethyldisilazane, a white precipitate began to form. The three necks were then equipped with a glass stopper, a reflux condenser fitted with a vacuum adaptor and a flow regulator, and a vacuum adaptor with a flow regulator, respectively. Once assembled and internally sealed, the flask was removed from the glovebox, connected to a Schlenk line, and refluxed at 125 °C for 3 h. During reflux, the solution appeared to turn pale yellow with no precipitate present. After reflux, the solution was cooled to room temperature and the reflux condenser was exchanged for a glass stopper. Volatiles were then removed by vacuum evaporation (evaporation removes not only the toluene but also the byproduct Me_3SiCl). The remaining solid after evaporation was white. While the flask was under vacuum, the solid was pumped back into the glovebox. It was then washed with diethyl ether (2×10 mL) and dried. Yield of dppa: 2.292 g, 64%. NMR spectroscopy of the isolated product matches that of the material purchased from a commercial vendor (Strem). ^{1}H NMR (500 MHz, CD_3CN): δ 4.33 (s, 1H, N−H), 7.33−7.38 (m, 20H, phenyls). $^{31}P\{^1H\}$ NMR (500 MHz, CD_3CN): δ 41.6 (s).

Preparation of Dicopper Precursor Complexes. Reported literature procedures for $[(\mu_2\text{-dppa})_2Cu_2(MeCN)_4][PF_6]_2$[16] and $[(\mu_2\text{-dcpm})_2Cu_2][PF_6]_2$[20] were used with the following modifications. In our hands, the reported procedure produced $[(\mu_2\text{-dppa})_2Cu_2(MeCN)_2][PF_6]_2$ with only two coordinated acetonitrile molecules rather than four, which was confirmed by ^{1}H NMR integration in DMSO-d_6. The molecular weight for $[(\mu_2\text{-dppa})_2Cu_2(MeCN)_2][PF_6]_2$ (1269.78 g mol^{-1}) was then used for all subsequent stoichiometric calculations. In the preparation of $[(\mu_2\text{-dcpm})_2Cu_2][PF_6]_2$, CH_2Cl_2 was used as the reaction solvent.

Preparation of $[(\mu_2\text{-dppa})_4Cu_4(\mu_4\text{-S})][PF_6]_2$ (2). $[(\mu_2\text{-dppa})_2Cu_2(MeCN)_2][PF_6]_2$ (1.00 g, 0.787 mmol) was added to a flask charged with acetone (30 mL) and a magnetic stir bar. In a separate vessel, Na_2S (0.0307 g, 0.393 mmol) was stirred in methanol (10 mL) until completely dissolved. The methanol solution of Na_2S was then added to the $[(\mu_2\text{-dppa})_2Cu_2(MeCN)_2][PF_6]_2$ solution dropwise, with stirring, at room temperature. Once all of the Na_2S solution had been added, the resulting deep-orange reaction mixture was stirred at room temperature for 3 h. The volume was reduced to 20 mL by vacuum evaporation, and then the solution was pipet-filtered through Celite to remove $NaPF_6$. The filtered solution was then completely evaporated and reconstituted in acetone (4 mL). Diethyl ether (approximately 10−12 mL) was slowly added, causing a bright-yellow precipitate to form. The yellow precipitate was collected by vacuum filtration and dried under vacuum. Yield of **2**: 0.593 g, 71%. Orange crystals may be obtained by dissolving yellow **2** in a minimum amount in acetone and allowing diethyl ether vapors to diffuse in through a pin-sized hole. ^{1}H NMR (500 MHz, acetone-d_6): δ 2.08 (s, coordinated acetone), 6.06 (s, N−H), 7.12−7.39 (m, 80H, phenyls). Note: Integration values for the N−H and coordinated solvent resonances were consistently lower than expected, possibly because of exchange processes with free solvent. $^{31}P\{^1H\}$ NMR (500 MHz, acetone-d_6): δ 36.6 (s, dppa), −145.8 (sept, J = 707.5 Hz, PF_6^-). FT-IR (cm^{-1}): 3297 (N−H), 3052, 1481, 1434, 1098, 832, 734, 688, 555, 521, 481. Anal. Calcd for $C_{96}H_{84}Cu_4F_{12}N_4P_{10}S$: C, 54.57; H, 3.97; N, 2.64. Found: C, 54.44; H, 4.08; N, 2.75. Note: The sample submitted for elemental analysis was dissolved in THF and then evaporated by vacuum three times to remove coordinated acetone molecules. Such a treatment was also used to prepare samples of **2** for further reactivity studies described below.

Preparation of $[(\mu_2\text{-dcpm})_3Cu_3(\mu_3\text{-S})][PF_6]$ (3). $[(\mu_2\text{-dcpm})_2Cu_2][PF_6]_2$ (1.00 g, 0.810 mmol) was dissolved acetone (30 mL) while stirring with a magnetic stir bar. In a separate vessel, Na_2S (0.042 g, 0.54 mmol) was stirred in methanol (7.5 mL) until completely dissolved. The Na_2S solution was then added dropwise at room temperature to the $[(\mu_2\text{-dcpm})_2Cu_2][PF_6]_2$ solution. Once the entire solution of Na_2S had been added, the resulting deep-amber reaction mixture was stirred at room temperature for 3 h. The solution was vacuum evaporated to approximately 5 mL and then pipet-filtered through Celite to remove $NaPF_6$. The resulting solution was then completely evaporated, and recrystallization was conducted using the same vapor diffusion method as that described for complex **2**. Yield of **3**: 0.472 g, 55%. ^{1}H NMR (400 MHz, DMSO-d_6): δ 1.12−1.40 (m, 60H, cyclohexyl), 1.62−1.98 (m, 72H, cyclohexyl). $^{31}P\{^1H\}$ NMR (500 MHz, acetone-d_6): δ −6.0 (s, dcpm), −146.8 (sept, J = 707.7 Hz, PF_6^-). FT-IR (cm^{-1}): 2920, 2846, 1444, 834, 754, 556, 513. Anal. Calcd for $C_{75}H_{138}Cu_3F_6P_7S$: C, 56.23; H, 8.73; N, 0.00. Found: C, 56.24; H, 8.47; N, 0.00.

Reaction between 2 and NaN_3. A solution of **2** (0.013 g, 0.0061 mmol) was prepared in THF (1 mL). In a separate vessel, NaN_3 (0.0039 g, 0.060 mmol) was dissolved in MeOH (1 mL). The NaN_3 solution was then added dropwise to the solution of **2** at room temperature with stirring. No immediate color change was observed. The solution appeared cloudy during initial drops of NaN_3 but was then completely clear once all NaN_3 had been added. Stirring was continued at room temperature for 16 h, during which time the reaction mixture became darker orange. The solution was then evaporated to dryness under vacuum, reconstituted in CD_2Cl_2, and then pipet-filtered through Celite to remove $NaPF_6$ and unreacted NaN_3. The column of Celite in the pipet was washed with a small amount of CD_2Cl_2 to capture as much product as possible. To the sample was added a solution of tri-*o*-tolylphosphine (200 μL of a 0.030 M solution in CD_2Cl_2, 0.0060 mmol) as a ^{31}P NMR internal standard. Yields based on quantitative ^{31}P NMR: **2′**, 51%; **4**: 19%; unreacted **2**, 8%. Crystals of **2′** and **4** were obtained by vapor diffusion of diethyl ether into a THF solution of the crude mixture in the same manner as that for complex **2**. ^{1}H NMR (400 MHz, CD_2Cl_2): δ 1.81 (m, 1.1H, coordinated THF), 2.37 (s, 8.8H, *o*-CH_3 in tri-*o*-tolylphosphine), 3.54 (s, 0.71H, N−H of **4**), 3.64 (s, integral not determined due to peak overlap, N−H of **2′**), 3.66 (m, integral not determined due to peak

dx.doi.org/10.1021/ic501720h | *Inorg. Chem.* 2014, 53, 10611−10619

overlap, coordinated THF), 6.69−7.37 (m, 60H, phenyls). $^{31}P\{^{1}H\}$ NMR (400 MHz, CD_2Cl_2): δ 40.3 (s, dppa of **4**), 38.6 (s, unknown), 36.7 (s, unreacted **2**), 35.4 (s, dppa of **2′**), −31.83 (s, tri-*o*-tolylphosphine), −146.09 (sept, J = 710.4 Hz, PF_6^-).

Preparation of $[(\mu_2\text{-dppa})_3Cu_3(\mu_3\text{-}N_3)_2][PF_6]$ (4) from N_3SiMe_3. To a solution of **2** (0.090 g, 0.042 mmol) in THF (3 mL) was added N_3SiMe_3 (56 μL, 0.42 mmol). No immediate color change or precipitate was observed. Stirring was continued at room temperature for 16 h, during which time the reaction color changed to dark red. The mixture was evaporated to dryness under vacuum. The red-brown residue was then reconstituted in THF (1 mL), and diethyl ether (1 mL) was added dropwise until a precipitate began to form. The tan precipitate was collected by vacuum filtration, washed with diethyl ether (2 × 3 mL), then dissolved in CH_2Cl_2 (2 mL), and pipet-filtered through Celite. The solution was then evaporated to dryness under vacuum. Crystals were obtained by vapor diffusion of diethyl ether into a THF solution in the same manner that as described for complex **2**. Yield of **4**: 0.0453 g, 68%. ^{1}H NMR (400 MHz, CD_2Cl_2): δ 3.61 (s, 3H, N−H), 7.09−7.33 (m, 63H, phenyls). $^{31}P\{^{1}H\}$ NMR (400 MHz, CD_2Cl_2): δ 40.30 (s, dppa), −146.12 (sept, J = 710.3 Hz, PF_6^-). FT-IR (cm^{-1}): 3274 (N−H), 3052, 2920, 2851, 2046 (N_3), 1481, 1434, 1303, 1099, 909, 833, 734, 691, 522, 481. Anal. Calcd for $C_{72}H_{63}Cu_3F_6N_9P_7$: C, 54.88; H, 4.03; N, 8.00. Found: C, 54.57; H, 4.07; N, 7.80.

Reaction between 2 and NaI. A solution of **2** (0.046 g, 0.0217 mmol) was prepared in THF (2 mL). In a separate vessel, NaI (0.0325 g, 0.218 mmol) was dissolved in MeOH (1 mL). The NaI solution was then added dropwise to the solution of **2** at room temperature with stirring. No immediate color change or precipitate was observed. The solution continued to stir at room temperature for 16 h, during which time the reaction mixture became darker orange after 16 h and was completely evaporated by vacuum. The solution was then evaporated to dryness under vacuum, reconstituted in CD_2Cl_2, and then pipet-filtered through Celite to remove $NaPF_6$ and unreacted NaI. The column of Celite in the pipet was washed with a small amount of CD_2Cl_2 to capture as much product as possible. To the sample was added a solution of tri-*o*-tolylphosphine (200 μL of a 0.216 M solution in CD_2Cl_2, 0.0216 mmol) as a ^{31}P NMR internal standard. Yields based on quantitative ^{31}P NMR: **6**, 75%; **5**, 13%. Crystals of **5** and **6** were obtained by vapor diffusion of diethyl ether into a THF solution of the crude mixture in the same manner as that for complex **2**. ^{1}H NMR (400 MHz, CD_2Cl_2): δ 1.81 (m, 2.1H, coordinated THF), 2.37 (s, 8.9H, *o*-CH_3 in tri-*o*-tolylphosphine), 3.65 (m, 2.1H, coordinated THF), 3.85 (s, 0.38H, N−H of **5**), 3.87 (s, 1.2H, N−H of **6**), 7.08−7.30 (m, 54.3H, phenyls). $^{31}P\{^{1}H\}$ NMR (400 MHz, CD_2Cl_2): δ 33.9 (s, dppa of **5**), 29.7 (s, dppa of **6**), −31.8 (s, tri-*o*-tolylphosphine), −146.1 (sept, J = 710.5 Hz, PF_6^-). Spectroscopic characterization was verified by toluene precipitation followed by washing of the solid with diethyl ether. The combined soluble fractions were predominantly **5**, while the solid fraction was predominantly **6**. Characterization of **6**. ^{1}H NMR (400 MHz, CD_2Cl_2): δ 1.81 (m, 2H, coordinated THF), 3.56 (s, 3H, N−H), 3.66 (m, 2H, coordinated THF), 7.08−7.30 (m, 60H, phenyls). $^{31}P\{^{1}H\}$ NMR (400 MHz, CD_2Cl_2): δ 29.6 (s, dppa), −146.1 (sept, J = 710.3 Hz, PF_6^-). FT-IR (cm^{-1}): 3281 (N−H), 3051, 2921, 2852, 2120, 1481, 1433, 1099, 927, 836, 734, 691, 523, 481.

■ ASSOCIATED CONTENT

Ⓢ Supporting Information

Detailed electrochemical, photophysical, and crystallographic data. This material is available free of charge via the Internet at http://pubs.acs.org.

■ AUTHOR INFORMATION

Corresponding Author

*E-mail: npm@uic.edu.

Author Contributions

The manuscript was written through contributions of all authors. All authors have given approval to the final version of the manuscript.

Notes

The authors declare no competing financial interest.

■ ACKNOWLEDGMENTS

Prof. Preston Snee and Armen Shamirian assisted with fluorescence measurements and quantum yield calculations. Dr. Dan McIlheny assisted with NMR measurements. We are grateful to the colleagues of Prof. Gregory Hillhouse for sharing an unpublished version of their manuscript in preparation. Start-up funds to N.P.M. were provided by the Department of Chemistry, University of Illinois at Chicago.

■ REFERENCES

(1) Pauleta, S. R.; Dell'Acqua, S.; Moura, I. *Coord. Chem. Rev.* **2013**, *257*, 332−349.

(2) (a) Brown, K.; Tegoni, M.; Prudêncio, M.; Pereira, A. S.; Besson, S.; Moura, J. J.; Moura, I.; Cambillau, C. *Nat. Struct. Biol.* **2000**, *7*, 191−195. (b) Rasmussen, T.; Berks, B. C.; Sanders-Loehr, J.; Dooley, D. M.; Zumft, W. G.; Thomson, A. J. *Biochemistry* **2000**, *39*, 12753−12756.

(3) Pomowski, A.; Zumft, W. G.; Kroneck, P. M. H.; Einsle, O. *Nature* **2011**, *477*, 234−237.

(4) Johnston, E. M.; Dell'Acqua, S.; Ramos, S.; Pauleta, S. R.; Moura, I.; Solomon, E. I. *J. Am. Chem. Soc.* **2014**, *136*, 614−617.

(5) Gorelsky, S. I.; Ghosh, S.; Solomon, E. I. *J. Am. Chem. Soc.* **2006**, *128*, 278−290.

(6) Bar-Nahum, I.; Gupta, A. K.; Huber, S. M.; Ertem, M. Z.; Cramer, C. J.; Tolman, W. B. *J. Am. Chem. Soc.* **2009**, *131*, 2812−2814.

(7) (a) Di Francesco, G. N.; Gaillard, A.; Ghiviriga, I.; Abboud, K. A.; Murray, L. J. *Inorg. Chem.* **2014**, *53*, 4647−4654. (b) Zhai, J.; Hillhouse, G. L. Manuscript in preparation. (c) Gourlay, C.; Nielsen, D. J.; White, J. M.; Knottenbelt, S. Z.; Kirk, M. L.; Young, C. G. *J. Am. Chem. Soc.* **2006**, *128*, 2164−2165. (d) Liu, H.; Tan, A. L.; Mok, K. F.; Mak, T. C.; Batsanov, A. S.; Howard, J. A.; Hor, T. S. A. *J. Am. Chem. Soc.* **1997**, *119*, 11006−11011. (e) Delgado, S.; Sanz Miguel, P. J.; Priego, J. L.; Jiménez-Aparicio, R.; Gómez-García, C. J.; Zamora, F. *Inorg. Chem.* **2008**, *47*, 9128−9130.

(8) Selected references featuring copper clusters with multiple μ_4-S ligands: (a) Khadka, C. B.; Najafabadi, B. K.; Hesari, M.; Workentin, M. S.; Corrigan, J. F. *Inorg. Chem.* **2013**, *52*, 6798−6805. (b) Lee, Y.; Sarjeant, A. A. N.; Karlin, K. D. *Chem. Commun.* **2006**, 621. (c) Dehnen, S.; Schäfer, A.; Fenske, D.; Ahlrichs, R. *Angew. Chem., Int. Ed. Engl.* **1994**, *33*, 746−749.

(9) Selected references featuring copper clusters with multiple μ_3-S ligands: (a) York, J. T.; Bar-Nahum, I.; Tolman, W. B. *Inorg. Chem.* **2007**, *46*, 8105−8107. (b) Lang, J.-P.; Tatsumi, K. *Inorg. Chem.* **1998**, *37*, 160−162. (c) Betz, P.; Krebs, B.; Henkel, G. *Angew. Chem., Int. Ed. Engl.* **1984**, *23*, 311−312.

(10) Selected references: (a) Yam, V. W.-W.; Lo, K. K.-W.; Fung, W. K.-M.; Wang, C.-R. *Coord. Chem. Rev.* **1998**, *171*, 17−41. (b) Wang, C.-R.; Lo, K. K.-W.; Fung, W. K.-M.; Yam, V. W.-W. *Chem. Phys. Lett.* **1998**, *296*, 505−514. (c) Yam, V. W.-W.; Lee, W.-K.; Lai, T.-F. *J. Chem. Soc., Chem. Commun.* **1993**, 1571. (d) Yang, R. N.; Sun, Y. A.; Hou, Y. M.; Hu, X. Y.; Jin, D. M. *Inorg. Chim. Acta* **2000**, *304*, 1−6.

(11) York, J. T.; Bar-Nahum, I.; Tolman, W. B. *Inorg. Chim. Acta* **2008**, *361*, 885−893.

(12) Chen, P.; Cabrito, I.; Moura, J. J. G.; Moura, I.; Solomon, E. I. *J. Am. Chem. Soc.* **2002**, *124*, 10497−10507.

(13) Lam, W. H.; Cheng, E. C.-C.; Yam, V. W.-W. *Inorg. Chem.* **2006**, *45*, 9434−9441.

(14) Selected references: (a) Lacy, D. C.; Park, Y. J.; Ziller, J. W.; Yano, J.; Borovik, A. S. *J. Am. Chem. Soc.* **2012**, *134*, 17526−17535. (b) Okamura, T.-A.; Ushijima, Y.; Omi, Y.; Onitsuka, K. *Inorg. Chem.*

2013, *52*, 381−394. (c) Tolman, W. B. *Inorg. Chem.* **2013**, *52*, 7307−7310.
(15) Haltia, T.; Brown, K.; Tegoni, M.; Cambillau, C.; Saraste, M.; Mattila, K.; Djinovic-Carugo, K. *Biochem. J.* **2003**, *369*, 77−88.
(16) Liu, H.; Calhorda, M. J.; Drew, M. G. B.; Felix, V.; Novosad, J.; Veiros, L. F.; de Biani, F. F.; Zanello, P. *J. Chem. Soc., Dalton Trans.* **2002**, 4365−4374.
(17) Han, L.; Shi, L.-X.; Zhang, L.-Y.; Chen, Z.-N.; Hong, M.-C. *Inorg. Chem. Commun.* **2003**, *6*, 281−283.
(18) τ_4 is a geometry index for four-coordinate centers, calculated to be 0 for square-planar geometries and 1 for tetrahedral geometries. See: Yang, L.; Powell, D. R.; Houser, R. P. *Dalton Trans.* **2007**, 955−964.
(19) Because both **1** and **2** are thermodynamically competent to reduce O_2 according to their redox potentials, we propose that kinetic binding of O_2 through the use of hydrogen bonds is the operative factor.
(20) Che, C.; Mao, Z.; Miskowski, V. M.; Tse, M. C.; Chan, C. K.; Cheung, K. K.; Phillips, D. L.; Leung, K. H. *Angew. Chem., Int. Ed.* **2000**, *39*, 4084−4088.
(21) Selected examples for comparison (cathodic shift of 0.47 V for dppa versus dppm when compared on the same potential scale): (a) Simón-Manso, E.; Kubiak, C. P. *Organometallics* **2005**, *24*, 96−102. (b) DeLaet, D. L.; Del Rosario, R.; Fanwick, P. E.; Kubiak, C. P. *J. Am. Chem. Soc.* **2001**, *109*, 754−758.
(22) (a) Berry, J. F. *Chem.—Eur. J.* **2010**, *16*, 2719−2724. (b) Sarangi, R.; Yang, L.; Winikoff, S. G.; Gagliardi, L.; Cramer, C. J.; Tolman, W. B.; Solomon, E. I. *J. Am. Chem. Soc.* **2011**, *133*, 17180−17191. (c) Sarangi, R.; York, J. T.; Helton, M. E.; Fujisawa, K.; Karlin, K. D.; Tolman, W. B.; Hodgson, K. O.; Hedman, B.; Solomon, E. I. *J. Am. Chem. Soc.* **2008**, *130*, 676−686.
(23) Bockman, T. M.; Kochi, J. K. *J. Org. Chem.* **1990**, *55*, 4127−4135.
(24) Pavlishchuk, V. V.; Addison, A. W. *Inorg. Chim. Acta* **2000**, *298*, 97−102.
(25) On the basis of the fact that fully reduced Cu_Z cannot be accessed by methyl viologen reduction, this also serves as an upper limit on the $Cu^{II}Cu^{I}_3/Cu^{I}_4$ potential of Cu_Z.
(26) The UV−vis spectrum of **3** also features a shoulder at 229 nm and a maximum at 216 nm.
(27) Recent examples: (a) Tskhovrebov, A. G.; Solari, E.; Scopelliti, R.; Severin, K. *Organometallics* **2012**, *31*, 7235−7240. (b) Piro, N. A.; Lichterman, M. F.; Harman, W. H.; Chang, C. J. *J. Am. Chem. Soc.* **2011**, *133*, 2108−2111. (c) Lee, J.-H.; Pink, M.; Tomaszewski, J.; Fan, H.; Caulton, K. G. *J. Am. Chem. Soc.* **2007**, *129*, 8706−8707. (d) Pamplin, C. B.; Ma, E. S. F.; Safari, N.; Rettig, S. J.; James, B. R. *J. Am. Chem. Soc.* **2001**, *123*, 8596−8597.
(28) (a) Kiefer, G.; Jeanbourquin, L.; Severin, K. *Angew. Chem., Int. Ed.* **2013**, *52*, 6302−6305. (b) Jayarathne, U.; Parmelee, S. R.; Mankad, N. P. *Inorg. Chem.* **2014**, *53*, 7730−7737. (c) Esmieu, C.; Orio, M.; Torelli, S.; Le Pape, L.; Pécaut, J.; Lebrun, C.; Ménage, S. *Chem. Sci.* **2014**, doi:10.1039/C4SC01487A.
(29) Paraskevopoulos, K.; Antonyuk, S. V.; Sawers, R. G.; Eady, R. R.; Hasnain, S. S. *J. Mol. Biol.* **2006**, *362*, 55−65.
(30) Sheldrick, G. M. *Acta Crystallogr.* **2008**, *A64*, 112−122.
(31) Dolomanov, O. V.; Bourhis, L. J.; Gildea, R. J.; Howard, J. A. K.; Puschmann, H. *J. Appl. Crystallogr.* **2009**, *42*, 339−341.
(32) Magennis, S. W.; Parsons, S.; Pikramenou, Z. *Chem.—Eur. J.* **2002**, *8*, 5761−5771.